Contact acoustic nonlinearity and local damage resonance for the detection of kissing bonds in structural adhesive joints

Jacopo Brunetti [a], Weeliam Khor [b], Walter D'Ambrogio [a], Annalisa Fregolent [c], Francesco Ciampa [b],*

[a] *Department of Industrial and Information Engineering and Economics, University of L'Aquila, 67100 L'Aquila, Italy*
[b] *School of Mechanical Engineering Sciences, University of Surrey, GU2 7HX, Guildford, UK*
[c] *Department of Mechanical and Aerospace Engineering (DIMA), University of Rome La Sapienza, 00184 Rome, Italy*

ABSTRACT

Adhesively bonded joints are susceptible to contamination of surfaces during manufacture and environmental deterioration in real operating conditions. These may cause the generation of so-called "kissing bonds" that can dramatically alter the strength of the joint leading to premature failure. Nonlinear acousto-ultrasonic (AU) techniques have shown great potential for monitoring kissing bonds with piezoelectric sensors permanently installed on the structural joint, thus enabling online and *in-situ* inspection. This paper investigated the combined contact acoustic nonlinearity (CAN) and local damage resonance (LDR) effects in the presence of kissing bonds in adhesive joints. Experimental nonlinear AU tests showed the formation of LDR frequency down-shifts and "jumps" of the fundamental damage resonance in adhesively bonded aluminium joints, with the kissing bond located internally to the overlapping region between the two adherends. These results were supported by a theoretical model based on the solution of the nonlinear Duffing's equation, under the assumption that the debonded region is a damped nonlinear harmonic oscillator subject to harmonic forcing. The Harmonic Balance Method was used to solve the nonlinear differential problem, showing the generation of frequency down-shifts via the dependence of the ratio between the excitation and LDR frequencies with the amplitude of the fundamental damage resonance. Additionally, two-dimensional finite element simulations using a reduced order model based on the Craig-Bampton technique were carried out to support experimental AU tests for the identification of the LDR frequency and the generation of nonlinear resonance effects. Good agreement between analytical, numerical, and experimental results revealed that a monitoring approach combining CAN and LDR is an extremely efficient and sensitive tool for ensuring integrity and safety of structural adhesive joints.

1. Introduction

Adhesive bonding is the process of joining two surfaces together using glue, epoxy-based resins, or plastic agents either at direct contact or via a third material, e.g., an adhesive tape [1]. The bonding process generally occurs through the evaporation of a solvent or through curing via heat, time, or pressure. This joining technique is currently used across many industries including aerospace, automotive, wind energy and civil infrastructures since it offers greater advantages over traditionally mechanical fastening [2]. Advantages include (i) even distribution of stress loads, thereby reducing the stress on the joint, (ii) the capability of joining a huge variety of dissimilar materials such as metals and composites, (iii) enhanced fatigue life and (iv) lighter weight compared to, for example, welding and riveting, which involves the use of metal fasteners, screws and bolts. However, adhesives are susceptible to contamination of surfaces during manufacture and environmental deterioration such as water ingression and corrosion in real operating environments, which may cause the generation of so-called "kissing bonds (KBs)" [3,4]. In KBs, the adherend surface and adhesive are only weakly forming a bond or containing a thin layer of contaminant, which can dramatically alter the strength of the joint leading to premature failure. There is, therefore, a need to develop non-destructive evaluation (NDE) methods such as acousto-ultrasonic (AU), thermographic, eddy current and radiographic techniques for the accurate detection of KBs both immediately after the joint is manufactured and during *in-service* operations [5–8]. Nevertheless, some of these NDE systems are not sufficiently sensitive to weak bonds due to lack of separation at interfaces, with a typical adhesive layer thickness being around 100μm. For example, in linear pulse-echo AU methods, the acoustic impedance of KBs is very small due to minimal local changes in stiffness and therefore little or no elastic energy is reflected for detection. Moreover, NDE techniques require the structural component to be disassembled and inspected offline, thus causing the maintenance process being time-consuming, expensive and, therefore, inefficient.

In recent years, both AU- and impedance-based structural health monitoring (SHM) systems have been developed to enable permanent and online monitoring of KBs in adhesively bonded joints [9–12]. Amongst these SHM solutions, nonlinear AU techniques offer great potential for monitoring KBs with piezoelectric (PZT) transducers directly attached onto the monitored component, thus enabling online inspection [10,13]. Nonlinear AU methods – also known as Nonlinear Elastic Wave Spectroscopy (NEWS) techniques – typically measure nonlinear effects including harmonics and sidebands (modulated signals) generated from one or more excitation frequencies [14–16]. These nonlinear effects are caused by the interaction of elastic waves with the damage, which produces vibration-induced "rubbing" and "clapping" at debonded interfaces of the structural joint. Contact-type elastic effects have been more broadly defined within the framework of Contact Acoustic Nonlinearity (CAN) to include a new family of nonlinear elastic phenomena like hysteresis, instabilities, and chaotic dynamics observed in damaged materials [17]. One of these nonlinear phenomena has sparked the interest of the AU research community in the last few years, which involves the local decrease of stiffness at damage interfaces resulting in peculiar local resonance effects. Particularly, if the frequency of the excitation signal matches the local damage resonance (LDR) frequency, the vibrational amplitude of material nonlinear effects can increase considerably by nearly 20–40 dBV [18,19]. The combination of CAN and LDR nonlinear phenomena has shown to significantly enhance the efficiency and reliability to damage detection. For example, Delrue et al. [20] investigated the effects of nonlinear LDR to detect KBs in the form of delamination in composite materials. Authors numerically found out that a significant increase in defect nonlinearity can be observed when the excitation frequency is tuned to the LDR frequency. Recently, the concepts of CAN and LDR have also been used alongside NDE vibro-thermography (also known as thermosonics) to further improve material damage visualisation [21–23]. Solodov [24] analytically hypothesised and experimentally observed a substantial qualitative departure from classical nonlinear harmonic effects in damaged composites via the generation of frequency down-conversion (subharmonics) and shifts of the LDR frequency by varying the input amplitude. This finding was a breakthrough for the analysis of nonlinear resonance phenomena in damage materials since it differentiated from the well-established nonlinear ultrasonic spectroscopy (NRUS) method [25,26]. Whilst the LDR is a local effect that greatly depends upon the morphology of the crack, its location, and the nature of mechanical contact at interfaces, NRUS works on the principle that the resonance frequency of the whole structure shifts as the strength of the nonlinearity increases in the damaged material. Guizburg et al. [27] applied the theoretical framework of CAN-induced LDR to identify subharmonic frequencies in weakly adhesively bonded aluminium-alloy single lap joints (SLJs). In this work, the KB was located at one end of the overlapping region between the two adherend beams. Authors numerically and experimentally observed that by exciting the SLJ at the frequency that is double of the LDR frequency, a subharmonic response matching the LDR frequency could be generated at the debonded region. Carrino et al. [28] experimentally examined a SLJ configuration like that reported by Guizburg et al. [27] and further confirmed results on the generation of subharmonics by varying the dimensions of the debonding region through the combined CAN and LDR effects. They also introduced a new mathematical model for the generation of frequency components obtained from the superposition of harmonic waves in weakly bonded SLJs that they named as "beating frequencies".

However, despite significant efforts on understanding the phenomenology of combined CAN and LDR effects in damaged materials, there are still outstanding questions related to the material nonlinear elastic behaviour in the presence of KBs in adhesive joints. Particularly, how would the topology of the KB influence the nonlinear dynamic behaviour of the LDR frequency in adhesively bonded structures? Can CAN-induced LDR frequency shifts or other nonlinear phenomena be generated in weakly bonded joints? For the first time, this paper attempted to address these questions showing the formation of nonlinear dynamic effects like LDR frequency down-shifts and "jumps" of the fundamental damage resonance in adhesively bonded aluminium joints, with the KB located internally to the overlapping region between the two adherends. These nonlinear AU results were supported by a theoretical model based on the solution of the nonlinear Duffing's equation, under the assumption that the debonded region is a damped nonlinear harmonic oscillator subject to harmonic forcing. The Harmonic Balance Method (HBM) was used to solve the nonlinear differential problem [29], showing the generation of frequency down-shifts via the dependence of the ratio between the excitation and LDR frequencies with the amplitude of the fundamental damage resonance. Additionally, explicit transient simulations using a reduced order model obtained

from the Craig-Bampton reduction of a two-dimensional (2D) finite element (FE) model were performed to support the identification of the LDR frequency and validate experimental findings on the generation of nonlinear resonance effects. The layout of the paper is as follows: in Section 2, the analytical solution of on the nonlinear Duffing equation using the HBM is presented for the investigation of nonlinear LDR effects. Section 3 describes the experimental set-up, whilst Section 4 provides both modal and transient numerical FE simulations to support experimental nonlinear acoustic experiments for the identification of the LDR frequency and the generation on nonlinear resonance phenomena. Section 5 reports the results of nonlinear acoustic testing for the generation of CAN-induced local resonance damage effects in the adhesive joint with KB. Finally, the conclusions of this paper are presented in Section 6.

2. Theoretical model

NEWS techniques are a family of AU inspection methods enabling accurate sensing of cracks and damage at early stages of formation. They measure material nonlinear elastic effects including harmonics and sidebands of one or more driving frequencies, which are mathematically described by the anharmonic elastic theory from Landau and Lifshitz (also known as "classical" nonlinear elastic theory) [30]. In this theoretical model, the elastic nonlinearity is associated with the material's lattice anharmonicity, and the dynamics of the macroscopic elastic field is defined by the following equation,

$$\rho \frac{\partial^2 u}{\partial t^2} = \frac{\partial \sigma}{\partial x}, \tag{1}$$

where ρ is the mass density, u is the displacement, t is the time and x is the propagation direction. At the macro-scale, the constitutive relation between the stress, σ, and strain, ϵ, takes the form of the Taylor-series expansion,

$$\sigma = K_0 \left[1 + \beta_2 \epsilon + \beta_3 \epsilon^2 \right] \epsilon, \tag{2}$$

where $K_0 = \partial \sigma / \partial \epsilon$ is the linear elastic modulus and β_2 and β_3 are parameters of nonlinearity defined as $\beta_2 = \frac{\partial^2 \sigma}{\partial \epsilon^2} / 2K_0$ and $\beta_3 = \frac{\partial^3 \sigma}{\partial \epsilon^3} / 3! K_0$. According to Eq. (2), the stiffness, K_0, is a nonlinear function of the strain resulting in a local variation of the wave speed, which in turn leads to a waveform distortion and harmonics generation. Experimental research has further shown that high AU nonlinearity can be found in materials with contact-type defects such as cracks, delamination, and KBs [31]. For these types of flaws, a significant increase of the magnitude of harmonic frequencies has been observed against pure lattice anharmonicity effects defined by the classical nonlinear Landau's theory [24]. Hence, the material AU response in the presence of debonding, cracks and delamination can be modelled under the framework of contact acoustic nonlinearity (CAN), which assumes a lack of stiffness symmetry on the motion of crack interfaces under tensile ($\epsilon > 0$) and compressive ($\epsilon < 0$) strains, leading to crack opening and closing [17]. When the crack opens, the material stiffness, K_0, is reduced, whereas when the crack is closed, the linear stiffness K_0 is restored. The CAN model is mathematically described by the following stepwise stress-strain relation,

$$\sigma = K_0 \left[1 - H\left(\epsilon - \epsilon^0\right) \frac{\Delta K}{K_0} \right] \epsilon, \tag{3}$$

where H is the Heaviside unit-step function, ϵ^0 is the initial static contact strain and $\Delta K = K_0 - \frac{\partial \sigma}{\partial \epsilon}|_{\epsilon > 0}$ is the "stiffness modulation depth", which infers that for a compressive strain ($\epsilon < 0$) the stiffness at crack interfaces restores the material linear elasticity K_0. The
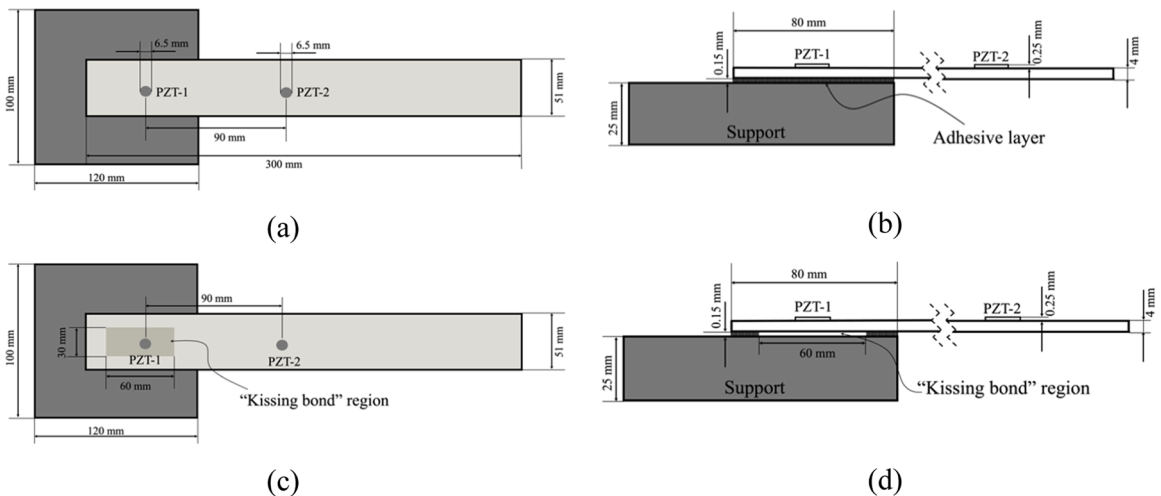

Fig. 1. Illustrations of adhesively bonded specimens. Top (a) and side (b) views of the perfectly bonded joint sample, and top (c) and side (d) views of the joint specimen with KB.

frequency spectrum of the CAN model displays higher harmonics modulated by the *sinc* envelope function, with the second harmonic mainly used for damage detection purposes. Moreover, as mentioned in the previous Section, the CAN framework also empowers further nonlinear elastic features experimentally observed in combination with the LDR phenomenon, including subharmonics and nonlinear dynamics effects. Depending on the location and nature of the debonded region, the combination of CAN and LDR can result in second harmonic generation of the fundamental resonance frequency as well as new elastic features typical of nonlinear resonances such as frequency down-shifts and the well-know "jump" effect, in which the response amplitude suddenly collapses at specific critical value of the excitation frequency. Whilst these nonlinear dynamics effects have been reported in damaged composites [24], to the best of authors' knowledge, they have never been observed in aluminium-alloy adhesive joints with KBs.

CAN-induced local resonance damage scenarios can be described mathematically using the following Duffing's dynamic equation, under the assumption that the debonded region is identified as a damped nonlinear oscillator subject to a harmonic force of amplitude coefficient, F_0, and angular frequency ω_0,

$$m\frac{\partial^2 u}{\partial t^2} + c\frac{\partial u}{\partial t} + ku + \gamma u^3 = F_0 cos(\omega_0 t), \tag{4}$$

with m the mass of the nonlinear oscillator, c the damping coefficient, k and γ the constant stiffness coefficients. The stiffness described by the term $ku + \gamma u^3$ has a linear part controlled by k and a nonlinear term dominated by γ, with $\gamma < 0$ (softening system). The quantity $\omega_D = \sqrt{k/m}$ from Eq. (4) is the fundamental angular resonance frequency associated with the debonded area, with the LDR frequency, f_D, simply equal to $\omega_D/2\pi$. Fig. 1 illustrates the geometrical configuration of the adhesive joint analysed in this work both in the case of perfect bonding (Fig. 1(a) and (b)) and with the KB located internally to the overlapping area between the aluminium beam and the support (Fig. 1(c) and (d)). Note that mathematical model of the nonlinear oscillator described by Eq. (4) is representative solely of the KB region as shown in Fig. 1(c) and (d).

Unlike previous works using the perturbation method to solve Eq. (4), see for example [19,24,27,28], in this paper, for the first time, the HBM was employed to analyse nonlinear LDR effects. Through the HBM, it was possible to mathematically reveal interesting resonance phenomena observed experimentally that are unique to nonlinear systems, such as downshifts of the LDR frequency by varying the excitation amplitude and the "jump" effect. By posing $\tau = \omega_D t$ and using the Chain Rule of the first and second derivative, Eq. (4) becomes,

$$\frac{d^2 u}{d\tau^2} + 2\zeta\frac{du}{d\tau} + u + \frac{\gamma}{k}u^3 = u_D cos(\Omega\tau), \tag{5}$$

with $\zeta = c/2m\omega_D$, $u_D = F_0/k$ and $\Omega = \omega_0/\omega_D$. Applying again the Chain Rule, Eq. (5) can be rewritten in the following non-dimensional form,

$$\frac{d^2 y}{d\tau^2} + 2\zeta\frac{dy}{d\tau} + y + \alpha y^3 = cos(\Omega\tau), \tag{6}$$

where $y = u/u_D$ and $\alpha = \gamma u_D^2/k$, with the coefficient α determining the nonlinearity of the system. The above second-order differential equation can be solved using the HBM [32], which uses a periodic solution in terms of Fourier series with limited numbers of harmonics and then, substitutes this solution into the dynamic Eq. (6) to find out balance of all harmonics. The periodic solution is of the form,

$$y = Ycos(\Omega\tau) + Zsin(\Omega\tau). \tag{7}$$

Substituting Eqs. (7) into (6) and neglecting harmonic terms of the frequency ratio, Ω, with index higher than the ansatz (>1), the following system of equations is obtained,

$$\left[(1-\Omega^2)Y + 2\zeta Z\Omega + \frac{3}{4}\alpha(Y^3 + YZ^2) - 1\right] = 0, \tag{8a}$$

$$\left[(1-\Omega^2)Z - 2\zeta Y\Omega + \frac{3}{4}\alpha(Z^3 + Y^2Z)\right] = 0. \tag{8b}$$

Transforming coefficients Y and Z in polar coordinates, i.e., $Y = a\,cos\theta$, $Z = a\,sin\theta$ and $Y^2 + Z^2 = A_D^2$, with A_D the amplitude of the fundamental LDR frequency, and substituting in the system of Eq. (8), after algebraic calculations yields,

$$\left[(1-\Omega^2) + \frac{3}{4}\alpha A_D^2\right]^2 A_D^2 + 4\zeta^2\Omega^2 A_D^2 = 1, \tag{9}$$

whose two solutions for Ω are,

$$\Omega_{1,2} = \left\{\frac{3}{4}\alpha A_D^2 + 1 - 2\zeta^2 \pm \frac{\sqrt{\Delta}}{A_D}\right\}^{\frac{1}{2}}, \tag{10}$$

with $\Delta = 4\zeta^4 A_D^2 + 1 - 4\zeta^2 A_D^2 - 3\alpha\zeta^2 A_D^4$. Assuming $\zeta^2 \ll 1$, Eq. (10) becomes,

$$\Omega_{1,2} \approx \left\{ \frac{3}{4}\alpha A_D^2 + 1 \pm \left[\frac{1}{A_D^2} - 4\zeta^2 \left(1 + \frac{3}{4}\alpha A_D^2 \right) \right]^{\frac{1}{2}} \right\}^{\frac{1}{2}}. \tag{11}$$

Eqs. (10) and (11) yield real values of $\Omega_{1,2}$ provided that $\Delta \geq 0$. Eq. (11) relates the frequency ratio, Ω, with the amplitude, A_D, of the LDR frequency. Such amplitude-frequency dependency of the fundamental resonance is known to change the shape of the A_D versus Ω curve and produce a fold-over (bending) effect. The jump-down frequency occurs when the peak amplitude is maximum, coinciding with the backbone curve given by $\Omega_b = \left(1 + \frac{3}{4}\alpha A_D^2\right)^{\frac{1}{2}}$. The amplitude at the jump-down frequency, A_{JD}, is determined by setting $\Delta = 0$ and rearranging terms. That is,

$$A_{JD} \approx \left\{ \frac{2}{3\alpha} \left[-1 + \left(1 + \frac{3\alpha}{4\zeta^2} \right)^{\frac{1}{2}} \right] \right\}^{\frac{1}{2}}. \tag{12}$$

Substituting Eq. (12) in the expression of Ω_b gives the equation for the jump-down frequency, Ω_{JD},

$$\Omega_{JD} \approx \frac{1}{\sqrt{2}} \left[1 + \left(1 + \frac{3\alpha}{4\zeta^2} \right)^{\frac{1}{2}} \right]^{\frac{1}{2}}. \tag{13}$$

For a softening system, α is negative and the term in the right inner brackets of Eq. (13) can become negative resulting in Ω_{JD} becoming complex. For Ω_{JD} to be real, it is necessary that $\alpha \geq \alpha_m$ with $\alpha_m = -4/3\zeta^2$. Fig. 2 illustrates the fold-over of the amplitude-frequency response curve (Eq. (11)) for two values of the nonlinear coefficient α, i.e., $\alpha = 0.9\alpha_m$ and $\alpha = 1.4\alpha_m$, in which the LDR frequency downshift and the jump effect are displayed. Similarly to Wawrzynski [33], a value of $\zeta = 0.02$ was used for the analytical model. The circle symbol and the dashed line in Fig. 2 correspond, respectively, to the jump-down frequency, A_{JD}, and the backbone curve, Ω_b, for the case of the nonlinear coefficient $\alpha = 0.9\alpha_m$.

3. Materials and experimental set-up

Adhesively bonded samples were manufactured using a 2024 aluminium alloy support joined to a beam of the same material through a layer 0.15 mm thick of epoxy resin (Araldite 2012A Epoxy Adhesive). Prior to bonding, the joint surfaces were polished with emery paper and cleaned with acetone. Mechanical properties of aluminium and adhesive materials are reported in Table 1, which were used for the numerical FE simulations as reported in Section 4.

Fig. 1(a)-(b) show the geometrical configuration of the adhesive joint in the case of perfect bonding, whereas the adhesively bonded specimen with a rectangular KB area of dimensions 60 mm x 30 mm is illustrated in Fig. 1(c) and (d). KB was "artificially" created during manufacturing by careful application of the epoxy adhesive and by placing a Teflon patch of the same thickness as the adhesive layer within the debonded region. After curing (16 h at 40 °C temperature), the Teflon patch was carefully removed. The aim of using Teflon was to reproduce contact-type defects of known dimensions internally to the bond line between the support and the aluminium beam for triggering CAN-induced LDR effects. The use of a Teflon patch to simulate controlled artificial damage is typical of NDE applications, with numerous examples available in literature [34,35]. For example, Ciampa et al. [36] used a Teflon patch to reproduce delamination and barely visible impact damage (BVID) in carbon-epoxy composites. As reported above, the location of the KB internal to the overlapping region between adherends was specifically chosen to analyse nonlinear resonance phenomena caused by the adhesion failure at the interface between the epoxy layer and the aluminium alloy, which may occur in practical applications either by poor quality of metal surfaces preparation or during the bonding process. The internal location of the KB would make impossible its detection via simple visual inspection. For the NEWS experimental campaign, two circular PZT transducers (PIC 255 000,053,020 from Physik Instrumente) with the diameter of 6.5 mm and thickness of 0.25 mm were surface glued onto the aluminium beam far away 90
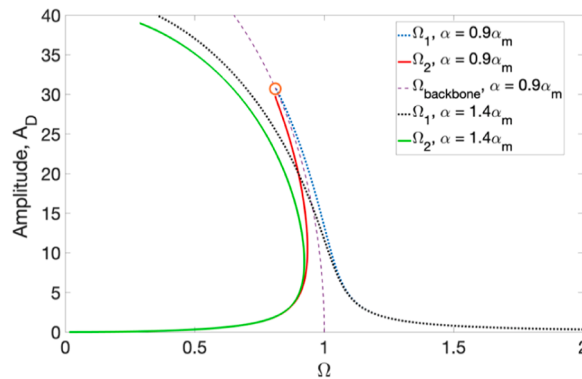
Fig. 2. Typical frequency-response curves of a Duffing oscillator obtained using Eq. (11). The LDR frequency downshift and "jump" nonlinear effects are generated by varying the nonlinear coefficient α.

Table 1
Mechanical properties of aluminium specimens and the epoxy adhesive layer.

Material	Young's modulus (GPa)	Mass density (Kg/m^3)	Poisson's ratio
2024 Aluminium alloy	72	2770	0.33
Araldite 2012A Epoxy Adhesive [27]	1.65	1350	0.31

mm from their geometric centres to generate and receive acoustic signals for KB detection. Two experimental acoustic testing procedures were carried out with the support of numerical simulations on both fully bonded and debonded adhesive joints. The first set of experiments consisted of identifying the LDR frequency through tap testing, whereas in the single tone-burst (follow-up) testing procedure, acoustic signals at specific driving frequencies selected from the tapping test were transmitted into the joint to detect CAN-induce LDR effects. The tap testing involved gently hitting the aluminium beam with a tap hammer and passively recording the vibrational response using the sensor PZT 1 connected to a PicoScope 4424 data acquisition system (12 bits of resolution) at the sampling rate of 20 kHz, which was in turn linked to a PC (Fig. 1). The time history of vibrational signals on both perfectly bonded and debonded adhesive joints were then processed using MATLAB software to perform the Fast Fourier Transform (FFT) algorithm and compute the power spectral density (PSD), which in turn revealed amplitude peaks associated to material's resonances. The basis for the tapping process is that a local change of material's stiffness would generate a local "amplification" of vibrations at the KB location when the aluminium beam is tapped, thus causing a noticeable amplitude peak in the PSD with a more accurate identification of the LDR frequency. Since a priori-knowledge of the LDR frequency is not trivial, a thorough comparison of the measured frequency spectrum on perfectly bonded and debonded joints supported the LDR identification process, with FE modelling providing clear evidence of the fundamental damage resonance frequency at the debonded area (see Section 4 for further details).

Several frequency peaks displayed in the PSD from the tapping process were then selected for the single tone-burst testing procedure. A 50 cycles long sine tone-burst, $s(t)$, enclosed in a Hanning window $H(t)$, was transmitted by the transducer PZT-2 at each excitation frequency, f_0, chosen from the tapping test,

$$s(t) = A_f H(t) \sin(2\pi f_0 t) \tag{14}$$

with A_f being the input amplitude initially chosen at 50 V. The number of cycles was chosen to make sure that vibrational modes could reach the debonded area and generate nonlinear harmonic signals recorded by the PZT-1 sensor place onto the KB region. The PZT-2 transmitter was driven by an arbitrary signal generator (TTI 50 MHz Pulse Generator T6501) connected to a high-voltage amplifier (Falco Systems DC High Voltage WMA-300) as shown in Fig. 3. Similarly to the tapping test, the transducer PZT-1 was linked to a PC via the PicoScope. Signals received by the piezoelectric sensor were sampled at 40 kHz with an acquisition window, $\tau = 0.5$ s. Time histories were averaged 20 times for each input frequency to improve the signal-to-noise ratio of measured waveforms. Key parameters used in both ultrasonic tap and single tone-burst tests are summarised in Table 2.

The purpose for single tone-burst experiments was to verify that second harmonic generation and CAN-induced nonlinear resonance effects only occur when the input frequency f_0 matched the LDR frequency, f_D, as mathematically conceived in Section 2.

4. Numerical simulations

Both structural modal and transient FE numerical simulations were performed using the commercial ANSYS and MATLAB software to support experimental nonlinear acoustic testing in Section 5, particularly on the identification of the LDR mode and the analysis of nonlinear resonance effects. Indeed, it is well-known that the LDR frequency can only be estimated analytically for "artificial-type" defects like flat bottom holes under specific boundary conditions [18]. Modal simulations were carried out to verify the presence of a Local Linear Mode (LLM) in the adhesive joint with KB, whose half upward oscillation has been found to be representative of the LDR mode (see Section 4.1 for further details). Structural transient FE analysis using the Craig-Bampton technique and a frictionless
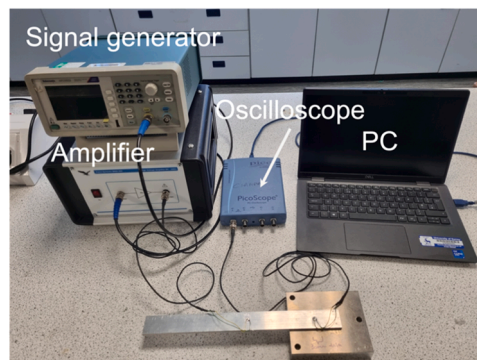
Fig. 3. Illustration of the nonlinear ultrasonic experimental set-up.

Table 2
Summary of key ultrasonic parameters used in both tap testing and single tone-burst experiments.

Parameter	Tap testing	Single tone-burst tests
Transmit frequency bandwidth	–	60 Hz – 10,000 Hz
Excitation cycles	–	50
Sampling frequency	20 kHz	40 kHz
Samples number	20,000	20,000

nonlinear contact bilinear model was developed, instead, to enable accurate identification of the LDR frequency and numerically display both higher (second) harmonics of the LDR frequency and amplitude-dependant shifts of the fundamental damage resonance.

### 4.1. Modal analysis for the local linear mode identification

Eigenvalues and their corresponding eigenfunctions were extracted from 2D solid models of fully bonded and de-bonded adhesive joints, which were created using a plane stress formulation of FE elements and geometrical dimensions as illustrated in Fig. 1. Fig. 4 shows the FE mesh consisting of an aluminium support bonded to an aluminium beam, whose properties are reported in Table 1, 702 plane stress elements and 2400 nodes were used to model the joint system.

The support was considered fixed at the bottom edge. Through modal simulations, it was possible to associate resonance frequencies with the corresponding modes of vibration for diverse solid models of adhesive joints, so that the LLM mode could be readily identified only in the presence of KB. An initial analysis was carried out under the hypothesis of perfect bonding between the two adherend parts. The lap joint was modelled by imposing a nodal coincidence between nodes of the beam and those of the support (Fig. 4 bottom left). In accordance with Fig. 1 and Section 2, a horizontal extension of 60 mm at the bond line of the joint was introduced to simulate the KB. FE nodes of the beam and the support were kept distinct without introducing any gap. A nodal coincidence was still assumed for those nodes located at the fully bonded regions of the joint (Fig. 4 bottom right). It should be noted that the proposed linear model enables only a global estimate of the system's vibrational response, since it does not simulate the interaction at the micro-scale (interface) between the beam and the support at the debonded region. Nevertheless, results on the system's natural frequencies (see the LLM frequency in Table 3) revealed the appearance of a local vibration mode at 5573 Hz, which was not observed in the perfectly bonded joint.

The top sub-plot of Fig. 5 illustrates that the mode shape associated to the LLM frequency of 5573 Hz has a bulge at the debonding area, which, in turn, produces a local increase of the vibrational amplitude. Owing to the linear modal analysis, the LLM of the debonded region also compenetrates the support, see the bottom sub-plot of Fig. 5. It should be highlighted that the nonlinear contact interaction at the KB location prevents, instead, such compenetration, thus yielding a nonlinear increase of the local stiffness, which causes a higher resonance frequency associated to the nonlinear LDR mode. As a result, whilts the upward half oscillation of the LLM can be used to visualise the mode shape of the LDR, the estimated value of the LDR frequency through this linear modal analysis is underrated. To enable a more accurate estimation of the LDR frequency and further assesses the LDR effect combined with CAN for the generation of nonlinear resonance phenomena at the KB location, a nonlinear contact bilinear model through a cubic contact pressure overclosure formulation was developed for the transient FE analysis of the adhesive joint, which is thoroughly reported in the next section.

4.2. Structural transient analysis for the identification of the LDR frequency and the generation of nonlinear effects

This section focuses exclusively on the modelling of the adhesively bonded joint with the KB. As anticipated in the previous Section, an accurate analysis of the mechanical behaviour of the joint at the debonded area requires a nonlinear dynamic model describing the contact between surfaces of the beam and the support at the overlapping region in the absence of the adhesive. Various analytical and numerical models have been developed in literature over the years to simulate nonlinear AU effects at the damage location, which have been thoroughly summarised by Broda et al. [37]. To name a few specifically for adhesively bonded joints, Ginzburg et al. [27] modified cohesive (interface) FE elements by introducing the so-called "mechanical diode crack model" of the KB, which used a
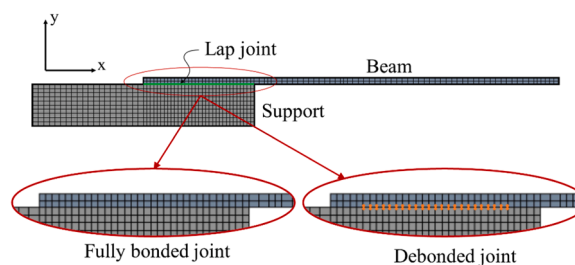
Fig. 4. Illustration of the plane stress FE model of the adhesively bonded joint, without (bottom left detail) and with (bottom right detail) KB. Geometrical dimensions for the support and the beam are reported in Fig. 1.

Table 3
System's natural frequencies of the adhesively bonded joint with and without the KB.

Mode	Frequency No KB [Hz]	Frequency with KB [Hz]
1	83	83
2	519	518
3	1451	1447
4	2832	2824
5	4649	4615
6	5256	5127
LLM	—	5573
7	6943	6935
8	9629	9605
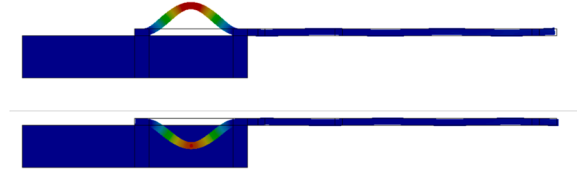
Fig. 5. Upward and downward half oscillations associated to the LLM frequency of 5573 Hz for the adhesive joint with the KB. Only the upward half oscillation of the mode shape can be associated to the LDR mode.

quadratic traction-displacement relationship to simulate sub-harmonics of the LDR frequency. In Carrino et al. [28], the debonded region was modelled by a frictionless contact bilinear law to account for nonlinear resonance phenomena occurring at the interface between adherends. In this paper, a cubic penalty pressure overclosure relationship is proposed for the frictionless contact (please see details as follows) to simulate second harmonic generation and amplitude-dependant frequency resonance shifts of the LDR frequency. Fig. 6 provides a graphical interpretation of the softening cubic contact pressure overclosure formulation proposed in this work.

For the numerical implementation, the well-known Craig-Bampton technique [38] was used to reduce the FE model of the adhesively bonded joint developed in the previous Section. The aim was to lower the computational burden of the numerical integration (characterised by several thousand of FE elements), whilst preserving physical degrees of freedom at interfaces between the beam and the support [39,40]. In the proposed model, FE nodes have been retained at locations where (i) the beam is excited, (ii) the material response is measured, and (iii) at the debonded area (see Fig. 7). Since nodal coincidence is not imposed at the debonded region of the joint, in the reduced model there are pairs of nodes on the beam and the support at the same identical location. The displacement of internal nodes is approximated using a limited number of fixed interface modes.

Once the FE model has been reduced (please see the Appendix for further mathematical details), the numerical integration of the material response is carried out using the Central Difference Method [41,42]. The dynamic equilibrium of the adhesively bonded joint with nonlinear elements at the interface can be expressed from Eq. (A.3) at a given time step i as,

$$\overline{M}\ddot{u}_i + \overline{C}\dot{u}_i + \overline{K}u_i + \overline{R}(\dot{u}_i, u_i) = \overline{F}_i^{ext}, \tag{15}$$

where $\overline{M}$, $\overline{C}$, and $\overline{K}$ represent the reduced mass matrix, the viscous damping matrix, and the stiffness matrix, respectively, $u_i(x, y, t)$ is the Craig Bampton displacement vector at time t_i [the subscript cb of Eq. (A.4) is here omitted for the sake of simplicity], $\overline{R}(\dot{u}_i, u_i)$ is the vector of the nonlinear contact forces and $\overline{F}_i^{ext}$ represents the external vector of dynamic loads. The terms $\dot{u}_i$ and $\ddot{u}_i$ are the velocity and acceleration vectors, respectively, which can be calculated using the Central Difference approximation with the integration time step h [39],

$$\dot{u}_i \simeq \frac{1}{2h}(u_{i+1} - u_{i-1}), \tag{16a}$$
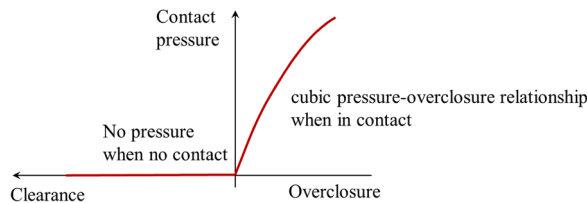
Fig. 6. Illustration of the softening cubic pressure overclosure relationship used for the frictionless contact to simulate second harmonic and nonlinear resonance effects of the LDR frequency.
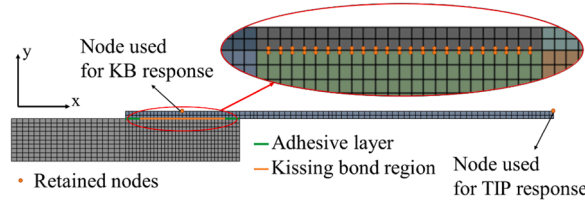
Fig. 7. Reduced FE model showing the location of retained nodes, which was used to obtain the material nonlinear response under single tone excitation.

$$\ddot{\boldsymbol{u}}_i \simeq \frac{1}{h^2}\left(\boldsymbol{u}_{i+1} - 2\boldsymbol{u}_i + \boldsymbol{u}_{i-1}\right). \tag{16b}$$

The dynamic equilibrium Eq. (15) can be rearranged to obtain the displacement, $\boldsymbol{u}$, at the time t_{i+1},

$$\boldsymbol{u}_{i+1} = \left[\frac{\overline{\boldsymbol{M}}}{\boldsymbol{h}^2} + \frac{\overline{\boldsymbol{C}}}{2\boldsymbol{h}}\right]^{-1}\left\{\left[\frac{2\overline{\boldsymbol{M}}}{\boldsymbol{h}^2} - \overline{\boldsymbol{K}}\right]\boldsymbol{u}_i + \left[\frac{\overline{\boldsymbol{C}}}{2\boldsymbol{h}} - \frac{\overline{\boldsymbol{M}}}{\boldsymbol{h}^2}\right]\boldsymbol{u}_{i-1} - \overline{\boldsymbol{R}}(\dot{\boldsymbol{u}}_i, \boldsymbol{u}_i) + \overline{\boldsymbol{F}}_i^{ext}\right\}. \tag{17}$$

Note that with this approach, the displacement at the time t_{i+1} is expressed as a function of the system's status in the previous time step. Only normal displacements of nodes (along the y-direction) at the contact line between the beam and the support are used for the contact problem. At the time t_i, the contact algorithm verifies the vertical overclosure of each pair of nodes on the beam (y_B) and the support (y_S) located at the overlapping region to calculate components R_B and R_S of the nonlinear contact force vector, $\overline{\boldsymbol{R}}$, according to the following formula,

$$\begin{cases} R_B = k_{lin}(y_S - y_B) + k_{nl}(y_S - y_B)^3 + c(\dot{y}_S - \dot{y}_B), & y_S - y_B > 0 \\ R_B = 0, & y_S - y_B < 0 \end{cases} \tag{18}$$

where $R_B = -R_S$ and k_{lin}, k_{nl} and c are the coefficient of linear contact stiffness, the coefficient of nonlinear contact stiffness and the contact damping coefficient, respectively. A graphical representation of Eq. (18) about the cubic penalty pressure overclosure relationship is shown in Fig. 6. Values of k_{lin}, k_{nl} and c parameters have been set in the model under the hypothesis that the penetration length at contact interfaces is less than 10^{-10} m. Note that, in analogy with the coefficient γ in Section 2, k_{nl} is also negative to account for material softening. The proposed numerical approach enables calculating the system's response to a harmonic excitation with a modest computational expense. The focus here is on the identification of the LDR frequency and the detection of higher (second) harmonics and nonlinear resonance effects in response to an excitation at the driving frequency, f_0, close to the LDR frequency, f_D. A numerical stepped sine excitation procedure in the frequency range 60 - 10,000 Hz, with a frequency step of 20 Hz, was initially numerically performed to confirm the actual resonance frequencies of the joint system and to identify the actual LDR frequency. The excitation acts at the midspan of the debonding area and the response is taken at two locations, the midspan of the debonding area and the tip of the beam. Fig. 8 shows the magnitude of the FRF at the two response locations. By looking at the FRF at the midspan of the debonding area [see black continuous line of Fig. 8], the LDR was found at about 8580 Hz. This is an expected result from the previous Section, since it has been highlighted that the LDR frequency must be higher than the LMM one. Note that the LDR peak does not appear on the FRF at the beam tip because the LDR mode has negligible displacement along the cantilever part of the beam, as shown in Fig. 5. This result also confirms that the damage resonance effect is a local phenomenon.

The spectrum of the steady-state harmonic response was then used to highlight the presence of second harmonics and nonlinear effects of the LDR frequency. For example, the stepped sine procedure around the frequency of 1447 Hz highlighted the presence of a vibrational mode, see the mode 3 in Table 3. The resonance frequency for this mode matched the frequency provided by the linear
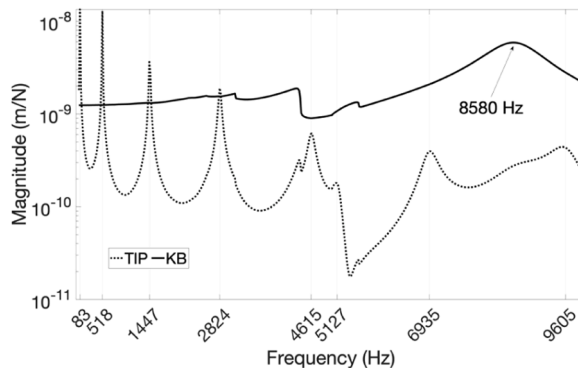

Fig. 8. Magnitude of the FRF in the frequency range 60 - 10,000 Hz at the beam tip (TIP) and at the midspan of the debonding area (KB).

modal analysis of Section 4.1, thus confirming that the proposed contact algorithm did not alter numerical simulations and the material acoustic response. Fig. 9 shows the magnitude of the frequency response function (FRF) around the resonance of 1447 Hz, which was achieved using a stepped sine simulation for an excitation force acting along the vertical direction on the tip of the beam.

When the stepped sine procedure was performed around the frequency of 8580 Hz, acoustic results highlighted the presence of a highly nonlinear mode. Fig. 10 shows the resonance peak shift of the magnitude of the FRF reconstructed using the stepped sine simulation by varying the excitation force, F^{ext}, which acts along the vertical direction on the debonded region of the joint. In agreement with the resonance effect illustrated by Eq. (10) in Section 2, the nonlinear pressure-overclosure relationship (Fig. 6) used in the FE simulation resulted in down-shifts of the resonance frequency by increasing the magnitude of the excitation force from 2×10^{-3} N to 6×10^{-3} N.

Fig. 11 shows the PSD normalised to the amplitude of the fundamental harmonic (excitation) frequency, $f_0 = f_D = 8580$ Hz. In this case, a steady-state material response was measured at nodes located on the top of the debonded region. Note that when the mode corresponding to the LDR frequency was excited by increasing the amplitude of the excitation frequency, the spectral response showed the presence of the second harmonic LDR mode and frequency shifts of both the LDR frequency - in agreement with the numerical stepped sine analysis illustrated in Fig. 10- and the second harmonic LDR mode.

5. Experimental results and discussions

As reported in Section 3, both fully bonded and debonded adhesive joints underwent both tapping tests and sinusoidal (harmonic) excitation, respectively, to identify experimentally the LDR frequency and nonlinear resonance effects such as second harmonics and frequency down-shifts by varying the input amplitude. The proposed two-stage testing process is analogous to that typically used in NEWS ultrasonic experiments in which input frequencies are initially selected from short or long sweep signals [21]. These driving frequencies are then transmitted into the damaged material using burst or continuous signals to detect nonlinear material effects. Fig. 12 shows the results of tapping tests on the fully bonded (Fig. 12(a)) and debonded (Fig. 12(b)) joints. A number of frequency peaks were identified from the material acoustic response measured by the sensor PZT-1, which resembled those observed in the numerical FE simulations of Section 4. Amongst these frequencies, only the frequency $f_0 = 8560$ Hz in the sample with KB significantly differentiated from those found in the perfectly bonded specimen.

Fig. 13 reports the nonlinear acoustic results of the long sine wave burst excitation transmitted by the transducer PZT-2 on the perfectly bonded joint for each driving frequency, f_0, chosen from the tapping tests. As expected, because of the perfectly bonded nature of the adhesive joint sample, none of these frequencies produced second harmonic generation. Fig. 14 illustrates the PSD results achieved from same type of harmonic analysis, but on the adhesive joint sample with KB. By selecting input frequencies from the tapping experiments as depicted in Fig. 12(b), a clear second harmonic frequency was measured by the sensor PZT-1 only for the input frequency, $f_0 = 8560$ Hz, which further proves this can be considered as the LDR frequency in accordance with results from the numerical FE analysis, see for comparison Figs. 11 and 14(d).

Further nonlinear acoustic experiments were carried out to assess CAN-induced LDR frequency shifts at the driving frequency, $f_D = 8560$ Hz. By varying the input amplitude from 50 V to 100 V, Fig. 15 shows a negative amplitude-dependant shift of LDR frequency (Fig. 15(a)), with $|\Delta f_D|/f_D = 2.9$ %, in addition to a sudden decrease ("jump") of both fundamental and second harmonic LDR frequencies at the threshold input amplitude of 80 V (Fig. 15(b)). As also found in Solodov et al. [24] in damaged composite materials, these effects are a consequence of the of the combined action of the defect nonlinearity and local resonance.

6. Conclusions

This paper explored the combined effect of CAN and LDR in adhesive joints with the KB located internally to the overlapping region between the two adherends. Results from numerical FE simulations using the Craig-Bampton technique and nonlinear AU experiments revealed that highly nonlinear dynamic effects of the fundamental and second harmonic LDR frequencies could be generated in
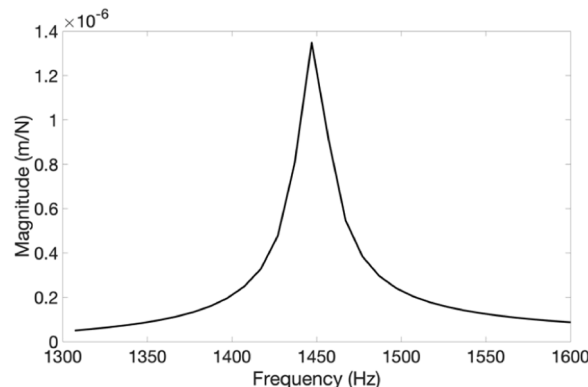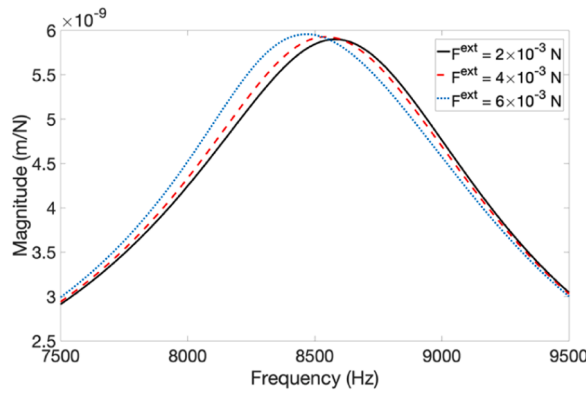

Fig. 9. Magnitude of the FRF around the resonance of 1447 Hz obtained using the stepped sine excitation procedure.

Fig. 10. Magnitude of the FRF around the resonance frequency of 8580 Hz obtained using the FE stepped sine excitation procedure for three different excitation forces. A nonlinear frequency shift is achieved by increasing the magnitude of the excitation force, thus highlighting nonlinear damage resonance effects at this specific resonance frequency.
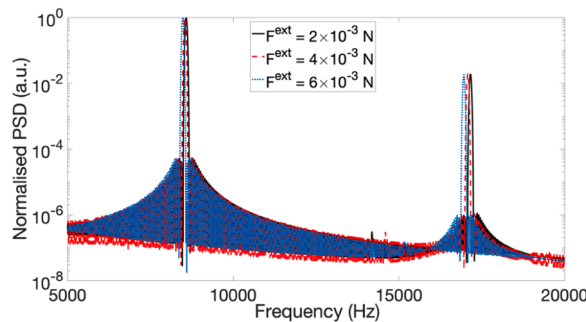
Fig. 11. Normalised PSD steady-state response at $f_0 = 8580$ Hz with three different excitation forces. In addition to the fundamental and second harmonic LDR modes, frequency shifts of both fundamental and second harmonic frequencies are numerically observed by increasing the magnitude of the excitation force.
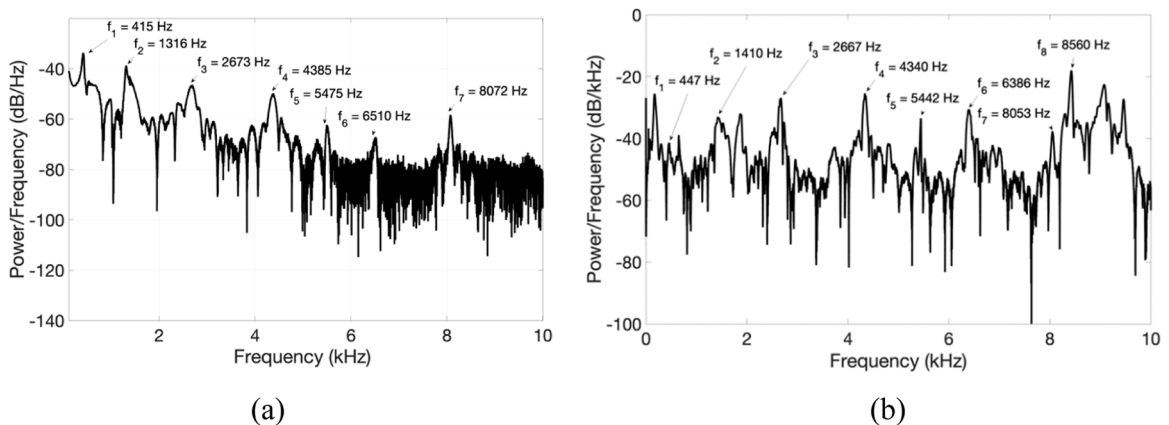
Fig. 12. PSD response with tap testing in the case of perfect adhesion (a) and debonded (b) samples.

debonded structural joints. Amplitude dependant down-shifts of the LDR frequency of ~2.9 % were observed in addition to a sudden collapse of both fundamental and second harmonic damage resonance frequencies at the threshold input amplitude of 80 V. These nonlinear resonance results were also in agreement with the solution of the nonlinear Duffing's differential equation using the Harmonic Balance Method. The simplicity of the combined CAN and LDR approach enables an easy implementation in a structural health monitoring system to reliably discriminate regions of poor adhesion in bonded joints. Finally, whilst this paper focused on the detection of KBs, further work is currently ongoing to identify the debonding location and assess its severity using sparse arrays of
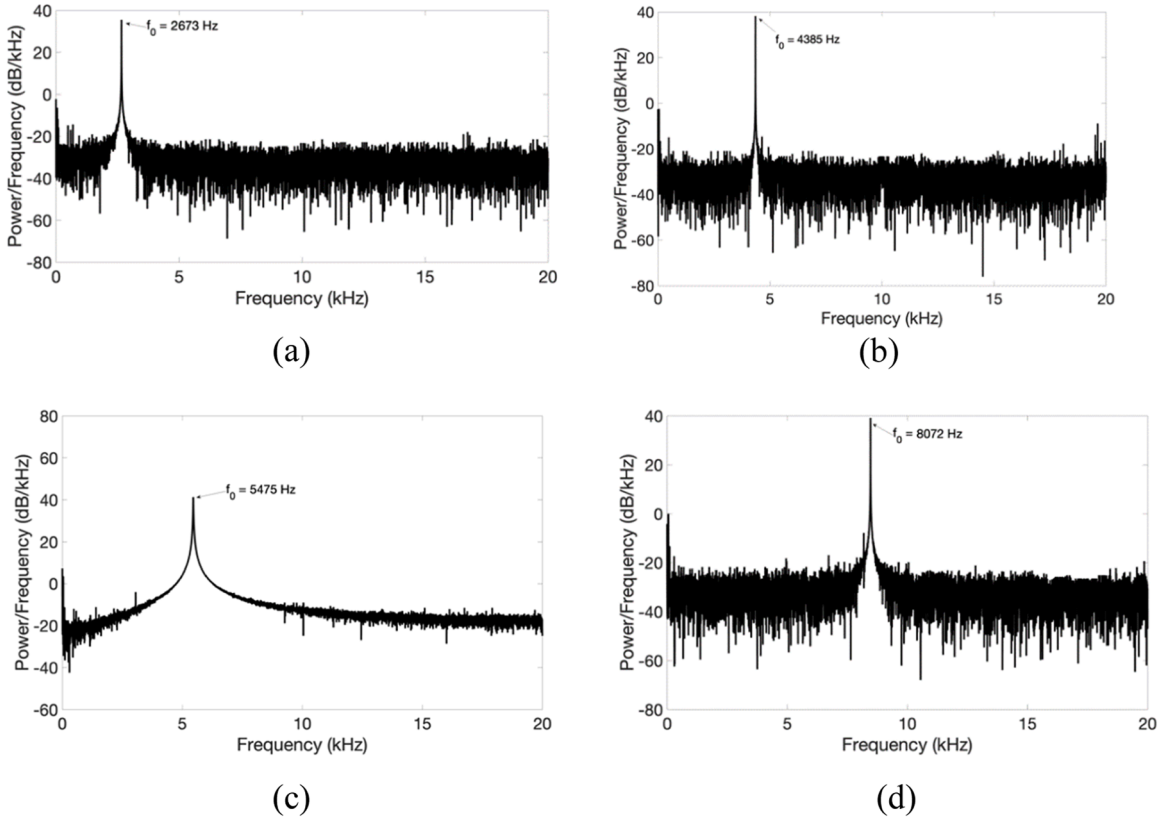
Fig. 13. Harmonic response measured in the adhesive joint sample with perfect bonding. Fundamental (input) frequencies were $f_0 = 2673$ Hz (a), $f_0 = 4385$ Hz (b), $f_0 = 5475$ Hz (c) and $f_0 = 8072$ Hz (d).

piezoelectric transducers.

CRediT authorship contribution statement

Jacopo Brunetti: Conceptualization, Methodology, Software, Writing – original draft. **Weeliam Khor:** Data curation, Visualization, Investigation. **Walter D'Ambrogio:** Supervision, Formal analysis, Resources, Writing – review & editing. **Annalisa Fregolent:** Supervision, Formal analysis, Writing – review & editing. **Francesco Ciampa:** Supervision, Conceptualization, Formal analysis, Resources, Writing – original draft.

Declaration of Competing Interest

The authors declare that they have no known competing financial interests or personal relationships that could have appeared to influence the work reported in this paper.

Data availability

The data that has been used is confidential.

Appendix

The Craig Bampton method is a method to reduce the size of the FE model. It provides a modal reduction of the system that accounts for both mass and stiffness, and the size of the reduced model depends on the frequency range [38],[40]. The equation of motion of a damped system with nonlinear forces depending on displacements and velocities, can be expressed as

$$\boldsymbol{M}\ddot{\boldsymbol{u}}(t) + \boldsymbol{C}\dot{\boldsymbol{u}}(t) + \boldsymbol{K}\boldsymbol{u}(t) + \boldsymbol{R}(\dot{\boldsymbol{u}}, \boldsymbol{u}) = \boldsymbol{F}^{ext}(t), \tag{A.1}$$

where $\boldsymbol{M}$ and $\boldsymbol{K}$ are the mass and stiffness matrices, $\boldsymbol{C}$ is the viscous damping matrix, $\boldsymbol{u}$ is the vector of displacement of all the physical
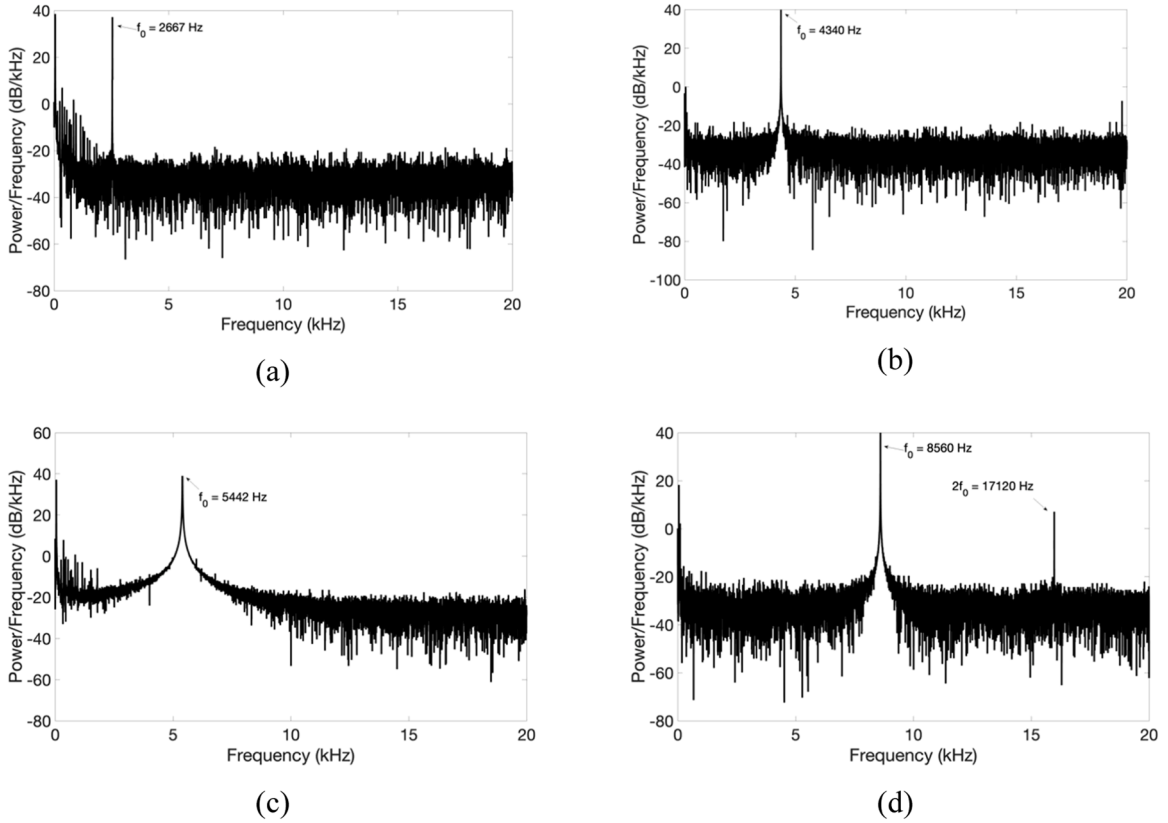
Fig. 14. Harmonic response in the adhesive joint with KB. Fundamental (input) frequencies were $f_0 = 2667$ Hz (a), $f_0 = 4340$ Hz (b), $f_0 = 5442$ Hz (c) and $f_0 = 8560$ Hz (d). Second harmonic is displayed at the LDR frequency, $f_D = 8560$ Hz.
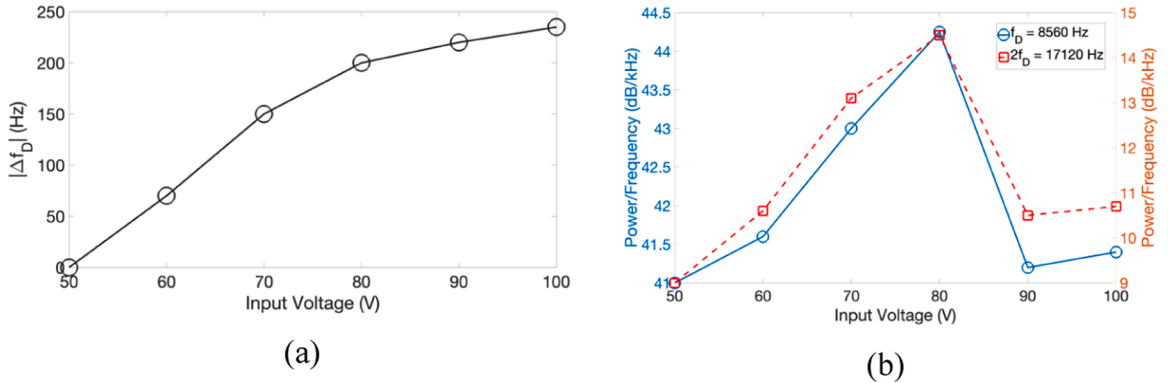
Fig. 15. Negative amplitude-dependant shift of the LDR frequency at $f_D = 8560$ Hz (a) and nonlinear amplitude dependence of f_D and $2f_D$ by varying the input voltage (b).

degrees of freedom of the finite element model, $R(\ddot{u}, u)$ is the vector of nonlinear forces, and, $F^{ext}(t)$, is the vector of applied forces. The global set of physical degrees of freedom, u, can be partitioned into two subsets: degree of freedoms (DoFs) that must be retained for further analysis, u_b, and internal DoFs, u_i, that can be reduced. Note that, the physical DoFs that are necessary to express the nonlinear forces must be retained. The Craig Bampton transform is defined as:

$$u = \begin{Bmatrix} u_b \\ u_i \end{Bmatrix} \cong \begin{bmatrix} I & 0 \\ \Phi_R & \Phi_I \end{bmatrix} \begin{Bmatrix} u_b \\ q \end{Bmatrix} = Tu_{cb}, \tag{A.2}$$

where T is the reduction matrix and u_{cb} is the reduced set of DoFs. The displacement u_i of internal DoFs can be expressed as the sum of

two terms,

- $\boldsymbol{\Phi_R u_b}$ that accounts for the displacement of internal DoFs due to the displacement of each boundary DoF, and $\boldsymbol{\Phi_R}$ is the matrix of static response modes.
- $\boldsymbol{\Phi_I q}$ is the displacement of internal DoFs due to the internal deformation expressed as a linear combination of fixed interface modes $\boldsymbol{\Phi_I}$ with coefficients $\boldsymbol{q}$ representing modal coordinates.

Therefore, since the number of modal coordinates is generally lower than the number of internal DoFs, the size of the problem in Eq. (A.1) can be reduced using Eq. (A.2) by means of the reduction matrix $\mathbf{T}$,

$$\boldsymbol{T^T M T \ddot{u}_{cb}}(t) + \boldsymbol{T^T C T \dot{u}_{cb}}(t) + \boldsymbol{T^T K T u_{cb}}(t) + \boldsymbol{T^T R(\dot{u}, u)} = \boldsymbol{T^T F^{ext}}(t) \tag{A.3}$$

with $\boldsymbol{T^T}$ the transpose of the matrix $\boldsymbol{T}$. From the previous equation, the reduced mass, damping, and stiffness matrices are obtained as $\overline{\boldsymbol{M}} = \boldsymbol{T^T M T}$, $\overline{\boldsymbol{C}} = \boldsymbol{T^T C T}$ and $\overline{\boldsymbol{K}} = \boldsymbol{T^T K T}$. Similarly, the vector of nonlinear forces becomes $\overline{\boldsymbol{R}}(\dot{u}, u) = \boldsymbol{T^T R}(\dot{u}, u)$ and the vector of applied forces becomes $\overline{\boldsymbol{F}}^{ext}(t) = \boldsymbol{T^T F^{ext}}(t)$. Therefore:

$$\overline{\boldsymbol{M}} \ddot{\boldsymbol{u}}_{cb}(t) + \overline{\boldsymbol{C}} \dot{\boldsymbol{u}}_{cb}(t) + \overline{\boldsymbol{K}} \boldsymbol{u}_{cb}(t) + \overline{\boldsymbol{R}}(\dot{u}, u) = \overline{\boldsymbol{F}}^{ext}(t) \tag{A.4}$$

If necessary, the displacement on the full set of DoFs, $\boldsymbol{u}$, can be obtained from the displacement on the reduced set, $\boldsymbol{u}_{cb}$, using the transformation in Eq. (A.2).

References

[1] L. Tong, G.P. Steven, Analysis and Design of Structural Bonded Joints, Kluwer Academic, Boston, 1999.
[2] R.D. Adams, Adhesive bonding: science, Technology and Applications, Woodhead Publishing, 2021.
[3] P.B. Nagy, Ultrasonic detection of kissing bonds at adhesive interfaces, J. Adhes. Sci. Technol. 5 (8) (1991) 619–630.
[4] D. Jiao, J.L. Rose, An ultrasonic interface layer model for bond evaluation, J. Adhes. Sci. Technol. 5 (8) (1991) 631–646.
[5] A. Tiwari, E.G. Henneke, J.C. Duke, Acousto-ultrasonic (AU) technique for assuring adhesive bond quality, J. Adhes. 34 (1–4) (1991) 1–15.
[6] B. Yılmaz, E. Jasiūnienė, Advanced ultrasonic NDT for weak bond detection in composite-adhesive bonded structures, Int. J. Adhes. Adhes. 102 (2020), 102675.
[7] R.C. Tighe, J.M. Dulieu-Barton, S. Quinn, Identification of kissing defects in adhesive bonds using infrared thermography, Int. J. Adhes. Adhesiv. 64 (2016) 168–178.
[8] I. Kryukov, S. Böhm, Prospects and limitations of eddy current shearography for non-destructive testing of adhesively bonded structural joints, J. Adhes. 95 (9) (2019) 874–886.
[9] Y. Zhuang, F. Kopsaftopoulos, R. Dugnani, F.K. Chang, Integrity monitoring of adhesively bonded joints via an electromechanical impedance-based approach, Struct. Health Monitor. 17 (5) (2018) 1031–1045.
[10] F. Amerini, M. Meo, Structural health monitoring of bolted joints using linear and nonlinear acoustic/ultrasound methods, Struct. Health Monitor. 10 (6) (2011) 659–672.
[11] G.M. Ramalho, A.M. Lopes, L.F. da Silva, Structural health monitoring of adhesive joints using Lamb waves: a review, Struct. Control Health Monitor. 29 (1) (2022) e2849.
[12] B.A. de Castro, F.G. Baptista, F. Ciampa, New imaging algorithm for material damage localisation based on impedance measurements under noise influence, Measurement 163 (2020), 107953.
[13] B.Y. Chen, S.K. Soh, H.P. Lee, T.E. Tay, V.B. Tan, A vibro-acoustic modulation method for the detection of delamination and kissing bond in composites, J. Compos. Mater. 50 (22) (2016) 3089–3104.
[14] K.E. Van Den Abeele, A. Sutin, J. Carmeliet, P.A. Johnson, Micro-damage diagnostics using nonlinear elastic wave spectroscopy (NEWS), Ndt & E Int. 34 (4) (2001) 239–248.
[15] J. Segers, S. Hedayatrasa, G. Poelman, W. Van Paepegem, M. Kersemans, Nonlinear local wave-direction estimation for in-sight and out-of-sight damage localization in composite plates, NDT & E Int. 119 (2021), 102412.
[16] G.R. Sherwood, D. Chronopoulos, A. Marini, F. Ciampa, 3D-printed phononic crystal waveguide transducers for nonlinear ultrasonic damage detection, Ndt & E Int. 121 (2021), 102456.
[17] I.Y. Solodov, N. Krohn, G. Busse, CAN: an example of nonclassical acoustic nonlinearity in solids, Ultrasonics 40 (1–8) (2002) 621–625.
[18] I. Solodov, J. Bai, S. Bekgulyan, G. Busse, A local defect resonance to enhance acoustic wave-defect interaction in ultrasonic nondestructive evaluation, Appl. Phys. Lett. 99 (21) (2011), 211911.
[19] F. Ciampa, G. Scarselli, M. Meo, On the generation of nonlinear damage resonance intermodulation for elastic wave spectroscopy, J. Acoust. Soc. Am. 141 (4) (2017) 2364–2374.
[20] S. Delrue, M. Tabatabaeipour, J. Hettler, K. van Den Abeele, Non-destructive evaluation of kissing bonds using local defect resonance (LDR) spectroscopy: a simulation study, Phys. Procedia 70 (2015) 648–651.
[21] G.P.M. Fierro, D. Ginzburg, F. Ciampa, M. Meo, Nonlinear ultrasonic stimulated thermography for damage assessment in isotropic fatigued structures, J. Sound Vib. 404 (2017) 102–115.
[22] I. Solodov, M. Rahammer, N. Gulnizkij, M. Kreutzbruck, Noncontact Sonic NDE and defect imaging via local defect resonance, J. Nondestruct. Eval. 35 (3) (2016) 48.
[23] A. Dyrwal, M. Meo, F. Ciampa, Nonlinear air-coupled thermosonics for fatigue micro-damage detection and localisation, NDT & E Int. 97 (2018) 59–67.
[24] I. Solodov, Resonant acoustic nonlinearity of defects for highly-efficient nonlinear NDE, J. Nondestruct. Evaluat. 33 (2014) 252–262.
[25] S. Maier, J.Y. Kim, M. Forstenhäusler, J.J. Wall, L.J. Jacobs, Noncontact nonlinear resonance ultrasound spectroscopy (NRUS) for small metallic specimens, NDT & E Int. 98 (2018) 37–44.
[26] E. Bozek, S. McGuigan, Z. Snow, E.W. Reutzel, J. Rivière, P. Shokouhi, Nonlinear resonance ultrasonic spectroscopy (NRUS) for the quality control of additively manufactured samples, NDT & E Int. 123 (2021), 102495.
[27] D. Ginzburg, F. Ciampa, G. Scarselli, M. Meo, SHM of single lap adhesive joints using subharmonic frequencies, Smart Mater. Struct. 26 (10) (2017), 105018.
[28] S. Carrino, F. Nicassio, G. Scarselli, Subharmonics and beating: a new approach to local defect resonance for bonded single lap joints, J. Sound Vib. 456 (2019) 289–305.
[29] M.J. Brennan, I. Kovacic, A. Carrella, T.P. Waters, On the jump-up and jump-down frequencies of the Duffing oscillator, J. Sound Vib. 318 (4–5) (2008) 1250–1261.

[30] L. Landau, E. Lifshitz, Mechanics, Vol. 1, CUP Archive, 1960.

[31] G. Scarselli, F. Ciampa, F. Nicassio, M. Meo, Non-linear methods based on ultrasonic waves to analyse disbonds in single lap joints, Proc. Inst. Mech. Eng., Part C: J. Mech. Eng. Sci. 231 (16) (2017) 3066–3076.

[32] A.H. Nayfeh, D.T. Mook, Nonlinear Oscillations, John Wiley & Sons, 2008.

[33] W. Wawrzynski, Duffing-type oscillator under harmonic excitation with a variable value of excitation amplitude and time-dependent external disturbances, Sci. Rep. 11 (1) (2021) 1–15.

[34] S.C. Wooh, C. Wei, A high-fidelity ultrasonic pulse-echo scheme for detecting delaminations in composite laminates, Compos. Part B: Eng. 30 (5) (1999) 433–441.

[35] G. Dua, R. Mulaveesala, P. Mishra, InfraRed image correlation for non-destructive testing and evaluation of delaminations in glass fibre reinforced polymer materials, Infrared Phys. Technol. 116 (2021) 103803.

[36] F. Ciampa, S.G. Pickering, G. Scarselli, M. Meo, Nonlinear imaging of damage in composite structures using sparse ultrasonic sensor arrays, Struct. Control Health Monitor. 24 (5) (2017) e1911.

[37] D. Broda, W.J. Staszewski, A. Martowicz, T. Uhl, V.V. Silberschmidt, Modelling of nonlinear crack–wave interactions for damage detection based on ultrasound—a review, J. Sound Vib. 333 (4) (2014) 1097–1118.

[38] D.J. Rixen, A dual Craig–Bampton method for dynamic substructuring, J. Comput. Appl. Math. 168 (1–2) (2004) 383–391.

[39] J. Brunetti, W. D'Ambrogio, A. Fregolent, Friction-induced vibrations in the framework of dynamic substructuring, Nonlinear Dyn. 103 (2021) 3301–3314.

[40] R.R. Craig Jr, M.C. Bampton, Coupling of substructures for dynamic analyses, AIAA J. 6 (7) (1968) 1313–1319.

[41] Warburton, G.B., 1995. Dynamics of Structures, by. Ray W. Clough and Joseph Penzien, McGraw-Hill, New York, 1993. No. of pages: 738. ISBN 0-07-011394-7.

[42] K.J. Bathe, Finite Element Procedures in Engineering Analysis, Prentice-Hall. Inc., Englewood Cliffs, NJ, 1982, p. 7632.